Laser and Particle Beams

cambridge.org/lpb

Scanning electron microscope studies on laser ablation of solids

Mohamed E. Shaheen[1], Joel E. Gagnon[2,3] and Brian J. Fryer[2,3]

[1]Department of Physics, Faculty of Sciences, Tanta University, Tanta, Egypt; [2]Great Lakes Institute for Environmental Research (GLIER), University of Windsor, Windsor, Ontario, N9B 3P4, Canada and [3]Department of Earth and Environmental Sciences, University of Windsor, Windsor, Ontario, N9B 3P4, Canada

Research Article

Cite this article: Shaheen ME, Gagnon JE, Fryer BJ (2019). Scanning electron microscope studies on laser ablation of solids. *Laser and Particle Beams* **37**, 101–109. https://doi.org/10.1017/S0263034619000132

Received: 28 July 2018
Revised: 21 January 2019
Accepted: 13 February 2019

Key words:
Brass; laser ablation; picosecond; sapphire; SEM

Author for correspondence:
Mohamed E. Shaheen, Department of Physics, Faculty of Sciences, Tanta University, Tanta, Egypt, E-mails: mshaheen73@science.tanta.edu.eg and mshaheen73@yahoo.com

Abstract

This study investigates the interaction of picosecond laser pulses with sapphire and brass in air using scanning electron microscopy. A picosecond laser system operating at a wavelength of 785 nm, pulse width of 110 ps, and variable repetition rate (1–1000 Hz) was used in this study. The pulse width applied in this work was not widely investigated as it lies in the gap between ultrashort (femtosecond) and long (nanosecond) pulse width lasers. Different surface morphologies were identified using secondary electron and backscattered electron imaging of the ablated material. Thermal ablation effects were more dominant in brass than in sapphire. Exfoliation and fractures of sapphire were observed at high laser fluence. Compared with brass, multiple laser pulses were necessary to initiate ablation in sapphire due to its poor absorption to the incident laser wavelength. Ablation rate of sapphire was lower than that of brass due to the dissipation of a portion of the laser energy due to heating and fracturing of the surface.

Introduction

The interaction of lasers with solid materials has been and continues to be an important topic in many areas of research (von der Linde and Sokolowski-Tinten, 2000; Gamaly *et al*., 2002; Nedialkov *et al*., 2004; Burakov *et al*., 2005; Ion, 2005; Brown and Arnold, 2010; Bäuerle, 2011; Shaheen and Fryer, 2012; Balling and Schou, 2013; Ganeev, 2014; Stafe *et al*., 2014; Shaheen *et al*., 2015*a*, 2016). Understanding the nature of these interactions is essential for selecting and matching a laser beam of specific properties to a particular application in order to achieve the desired outcomes. A comprehensive study of laser interactions with solids is not easy because laser–solid interactions involve many processes and many interfering parameters. In addition to the direct laser–solid interactions, plasma formation and expansion, as well as its subsequent interactions with the incident laser beam, increase the complexity of these processes (Bäuerle, 2011; Stafe *et al*., 2014; Shaheen *et al*., 2015*b*). A large number of parameters should be considered when investigating the interaction of lasers with different solid materials. Laser properties, such as fluence, pulse width, repetition rate, beam profile, number of laser pulses, and wavelength, are important parameters of a laser beam that controls the interaction processes (Hashida *et al*., 2002; Le Harzic *et al*., 2005; Bashir *et al*., 2013; Jelani *et al*., 2013; Akram *et al*., 2014; Shaheen *et al*., 2019). Add to this the physicochemical properties of the target material, such as thermal and electrical conductivity, reflectivity, absorption, and dielectric constant. The environment (vacuum or gas, gas type, and properties) in which laser–solid interactions take place is also important and cannot be neglected (Amoruso *et al*., 2005; Ali *et al*., 2013; Krstulović *et al*., 2013; Shaheen *et al*., 2013*a*, 2014; Dawood *et al*., 2015).

Numerous diagnostic techniques have been applied to study the interactions of lasers with solids (Bäuerle, 2011; Balling and Schou, 2013; Stafe *et al*., 2014). While many techniques have been developed for *in situ* real-time analysis, the most precise methods for investigating structural changes are those carried out after ablation is complete. Scanning electron microscopy is an important offline diagnostic technique, which can provide useful information about the ablation process. Surface morphology of the ablated structures and the shape of the ablated particles have been widely studied by scanning electron microscopy (Wilder-Smith *et al*., 1997; Kumar *et al*., 2011; Shaheen *et al*., 2016). A scanning electron microscope (SEM) provides two common imaging modes: secondary electrons (SE) and backscattered electrons (BSE), depending on the origin of electrons that are used to image the sample. In SE images, the electrons are ejected from the valence band or the conduction band in the sample (Williams and Carter, 2009). These electrons are not associated with a specific atom and therefore they do not give information about the chemical composition of the target material. SE are weak, can only escape from a layer within approximately 2 nm from the sample surface, and consequently can only be used to produce images of the target surface. BSE are more energetic than SE because they originate from the incident electron beam after being reflected or

© Cambridge University Press 2019

CAMBRIDGE UNIVERSITY PRESS

backscattered by the atoms in the interaction volume of the sample. The intensity of the BSE depends on the atomic number of the target material and therefore BSE can be used to detect changes in contrast between areas of different chemical composition (Williams and Carter, 2009).

Sapphire has many important applications in optical systems and semiconductor devices (Cui *et al.*, 2014). It is a relatively hard transparent material that is difficult to process using chemical or mechanical means due to its high chemical stability and hardness (Ashkenasi *et al.*, 1997; Horisawa *et al.*, 2004; Qi *et al.*, 2010; Shaheen *et al.*, 2015*b*). Direct ablation of sapphire or other transparent brittle materials with nanosecond infrared lasers is difficult and cannot produce precise, well-defined micrometer-sized craters because these lasers have relatively low photon energy and poor absorption by highly transparent materials. Application of lasers of high intensity (e.g., ultra-short pulse width lasers) or high photon energy [e.g., ultraviolet (UV) lasers] can improve the absorption and ablation quality of transparent materials (Zhou and Wu, 2010). Brass alloys are strong, corrosion resistant, conductive, and machinable. They are used in many important applications such as water pipes, heat exchangers, electrical wires, and marine engines. The physical properties of brass are fundamentally different from those of sapphire. This greatly affects the absorption of laser energy, the way of energy dissipation, and the mechanisms of material removal.

In this study, we make use of scanning electron microscopy to explore the nature of picosecond laser interactions with sapphire and brass by investigating the evolution of the surface morphology of craters produced at different laser operating conditions. The investigated laser has a pulse width (110 ps) intermediate between the most commonly used nanosecond and the most expensive femtosecond laser systems which are used in laser ablation applications.

Experimental

Laser ablation experiments were conducted at the University of Windsor, Windsor, Ontario, Canada using a femtosecond laser system that has been previously described in Shaheen *et al.* (2013*b*). All ablation experiments were performed in air under atmospheric pressure. The femtosecond laser system (Quantronix® Integra-C) was designed to emit two laser beams at a wavelength of 785 nm and a repetition rate of 1–1000 Hz. One of the beams is a femtosecond beam with a pulse width of 130 fs, and the other beam is a picosecond beam with a pulse width of 110 ps. Both beams can be used simultaneously, however, in this study the picosecond beam was used exclusively. The energy of the two laser beams can be varied from a few microjoules per pulse to a maximum of 2 mJ per pulse using a built-in half-wave plate and a polarizer. The laser energy was measured using an Ophir Nova II laser power/energy meter and a pyroelectric head PE-10 V2. A Newport® electronic shutter and digital exposure control were used to control the number of laser pulses to create craters using a pre-defined number of pulses. An Olympus® BX51 optical microscope equipped with a Prior Scientific® 3D stage (controlled by a Prior ProScan™ H31 controller) and a CCD camera was used to observe the ablation process, and to specify the ablation point and focus position of the laser beam. Crater morphology was characterized using a FEI Quanta® 200 FEG SEM. Sapphire, in the form of circular wafers of 3 mm thickness and 9.5 mm diameter, with random orientation (Esco Optics, New Jersey, USA) and brass [SRM 1107 naval brass B from National Institute of Standard and Technology (NIST), Gaithersburg, USA] were used as target materials for ablation by picosecond laser pulses. Sapphire and brass were selected in this study because they represent two different types of materials (i.e., dielectrics and conductors) which have different electrical, thermal, and optical properties. The ablation depth of craters were measured using an Olympus® BX51 optical microscope.

Results and discussion

Sapphire

Figure 1 shows the surface morphology of craters produced on sapphire at a repetition rate of 100 Hz and fluence of 2.3, 6.6, and 10.6 J/cm^2, using 20, 50, 100, and 200 laser pulses. The laser beam was focused on the target surface using a 10× magnification microscope objective lens (Olympus UMPlanFL, 0.3 numerical apertures). Under these experimental conditions, the smallest crater diameter (8 μm) was obtained at fluence of 2.3 J/cm^2. The craters were almost circular in shape and showed deposition of very fine particles on the surrounding sample surface. The crater depth and the amount of deposited materials were found to increase with increasing the laser fluence and number of laser pulses. At low fluence, cracks and fractures were not observed on the surface around the craters. Small surface cracks were observed at fluence of 6.6 J/cm^2 when the number of laser pulses exceeded 100. Melting and ejection of molten droplets were also observed at fluence of 6.6 and 106 J/cm^2 when the number of pulses exceeded 100 and 50 pulses, respectively. Cracks were observed on the sample surface at a lower number of laser pulses at laser fluence of 10.6 J/cm^2. This is illustrated in Figure 2, where high magnification images of craters produced at a fluence of 10.6 J/cm^{2}using 40 and 100 laser pulses are shown.

A distinct change in crater morphology was observed when ablation was conducted at higher fluence. Figure 3 shows the surface morphology of two carters produced at a fluence of 53 J/cm^2 using 20 and 100 laser pulses at a fixed repetition rate of 100 Hz. Most of the laser energy was consumed in exfoliating the surface at the interaction area. The crater produced by 20 laser pulses was poorly shaped and showed a shallow, irregular surface structure. At 100 laser pulses, a small crater was produced at the center of the exfoliated structure. At higher fluence, ablation efficiency was low due to the dissipation of laser energy in heating and fracturing the irradiated area.

It is worth mentioning that the optics used in a given experiment is a very important factor that affects ablation rate and crater morphology. Different ablation rates and crater morphology can be obtained by using different objective lenses to focus the laser beam on the target surface. Figure 4 shows SE images of craters produced on sapphire in air using a different microscope objective lens (Newport M-10x, 0.25 numerical aperture). The craters were produced at a fixed repetition rate of 100 Hz using 20 (Fig. 4a), 50 (Fig. 4b), 100 (Fig. 4c), and 500 (Fig. 4d) laser pulses at a fluence of 79.5 J/cm^2. The shape of the craters was found to vary with the number of laser pulses and fluence. Increasing the number of pulses gradually reduced the fractured area at the crater edge due to the gradual increase in the crater diameter (Fig. 4d). A single laser pulse was not able to induce ablation due to the poor absorption of sapphire to the incident laser wavelength. Application of multiple laser pulses to the same spot causes modification of the properties of sapphire at the irradiation area (Lenzner *et al.*, 1999). The modification and roughening of the surface by successive laser pulses enhance absorption to the

https://doi.org/10.1017/S0263034619000132 Published online by Cambridge University Press

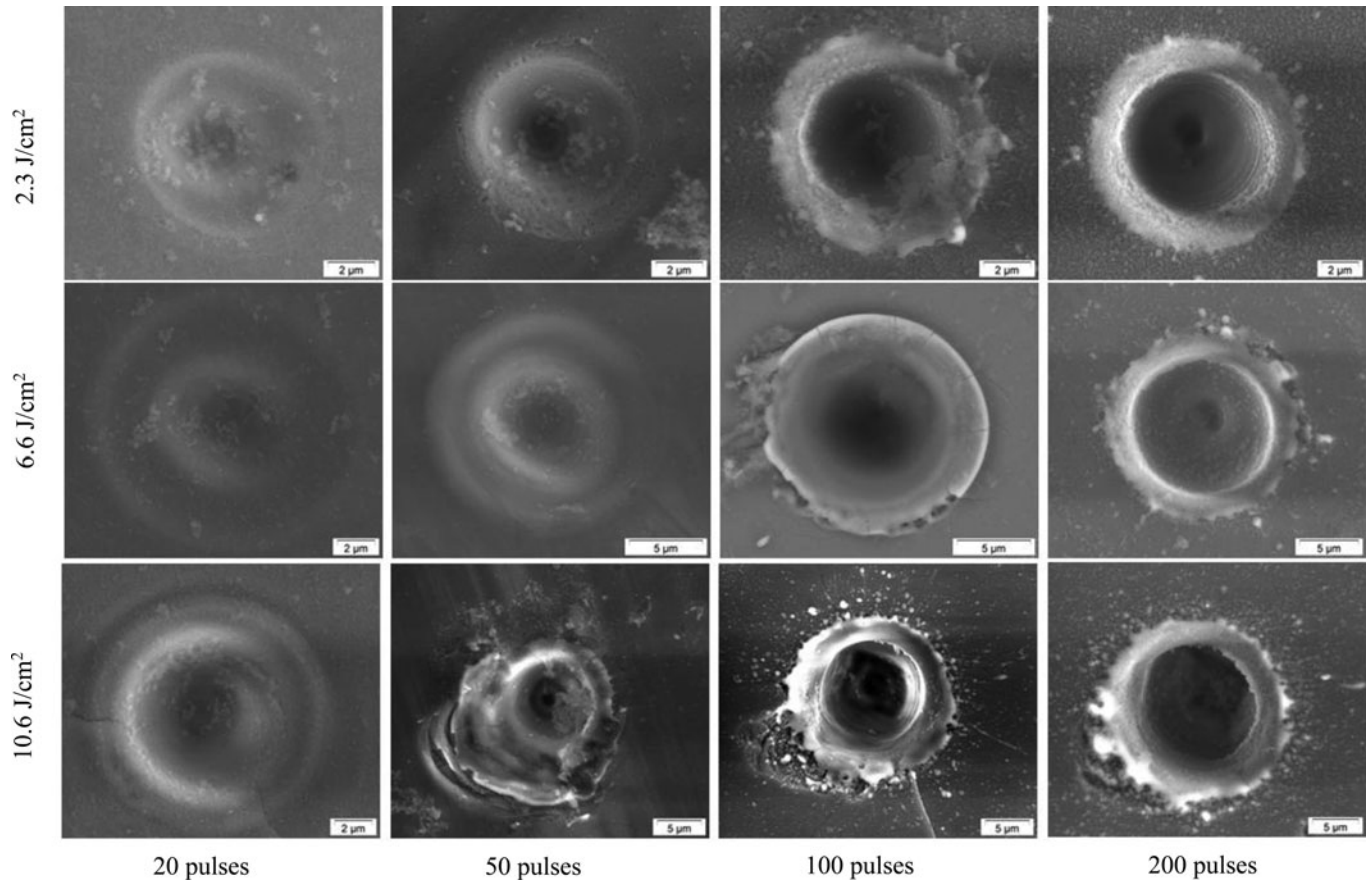


Fig. 1. Craters produced on sapphire at different laser fluence and number of laser pulses in air. Repetition rate was fixed to 100 Hz.

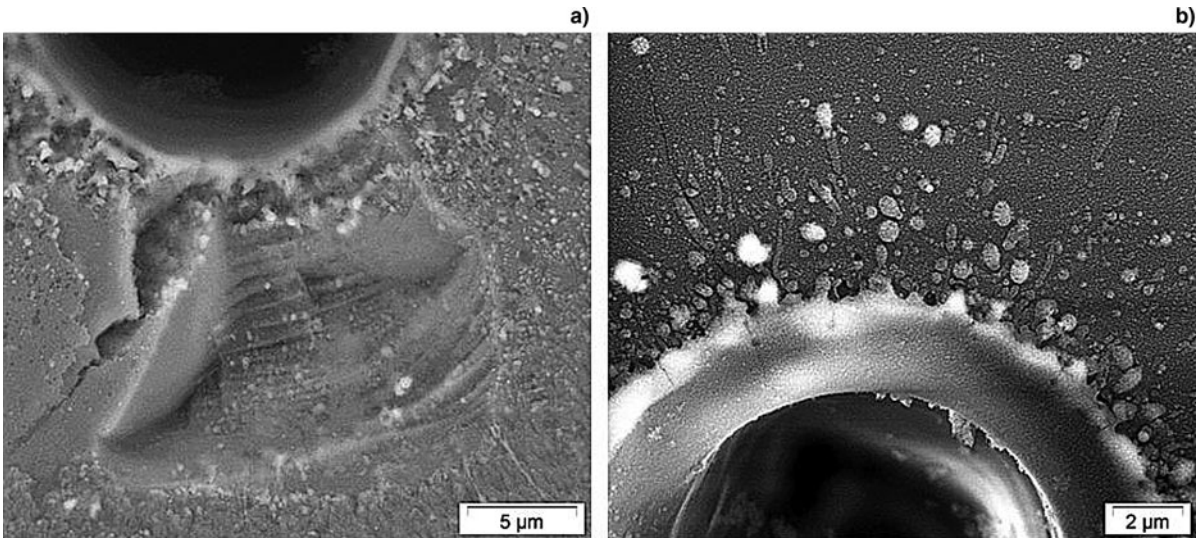


Fig. 2. A close-up image of craters produced on sapphire using 40 (a) and 100 (b) laser pulses at fluence of 10.6 J/cm^2.

incident radiation due to the formation of defects (color centers) and the generation of electronic states within the forbidden energy gap (Stuart *et al.*, 1996; Lenzner *et al.*, 1999; Bäuerle, 2011). The need for a certain number of laser pulses (incident at the same spot) to initiate ablation at a constant fluence is known as incubation (Hülsenberg *et al.*, 2008; Wu *et al.*, 2011). Increasing the fluence reduces the number of laser pulses required to initiate ablation.

The surface morphology of the craters produced on sapphire using multiple picosecond laser pulses varied with location of the crater on the surface (i.e., craters produced under similar conditions were not reproducible). This can be attributed to the basic

https://doi.org/10.1017/S0263034619000132 Published online by Cambridge University Press

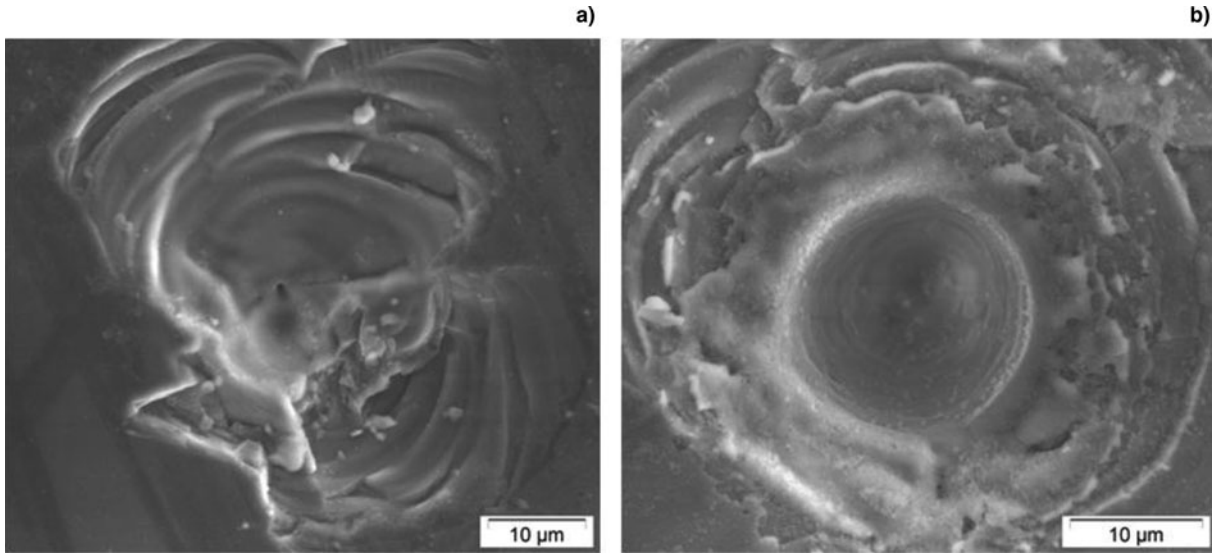


Fig. 3. Craters produced on sapphire at fluence of 53 J/cm^2 using 20 (Fig. 1a), 100 (Fig. 1b) laser pulses in air. Repetition rate was fixed to 100 Hz.

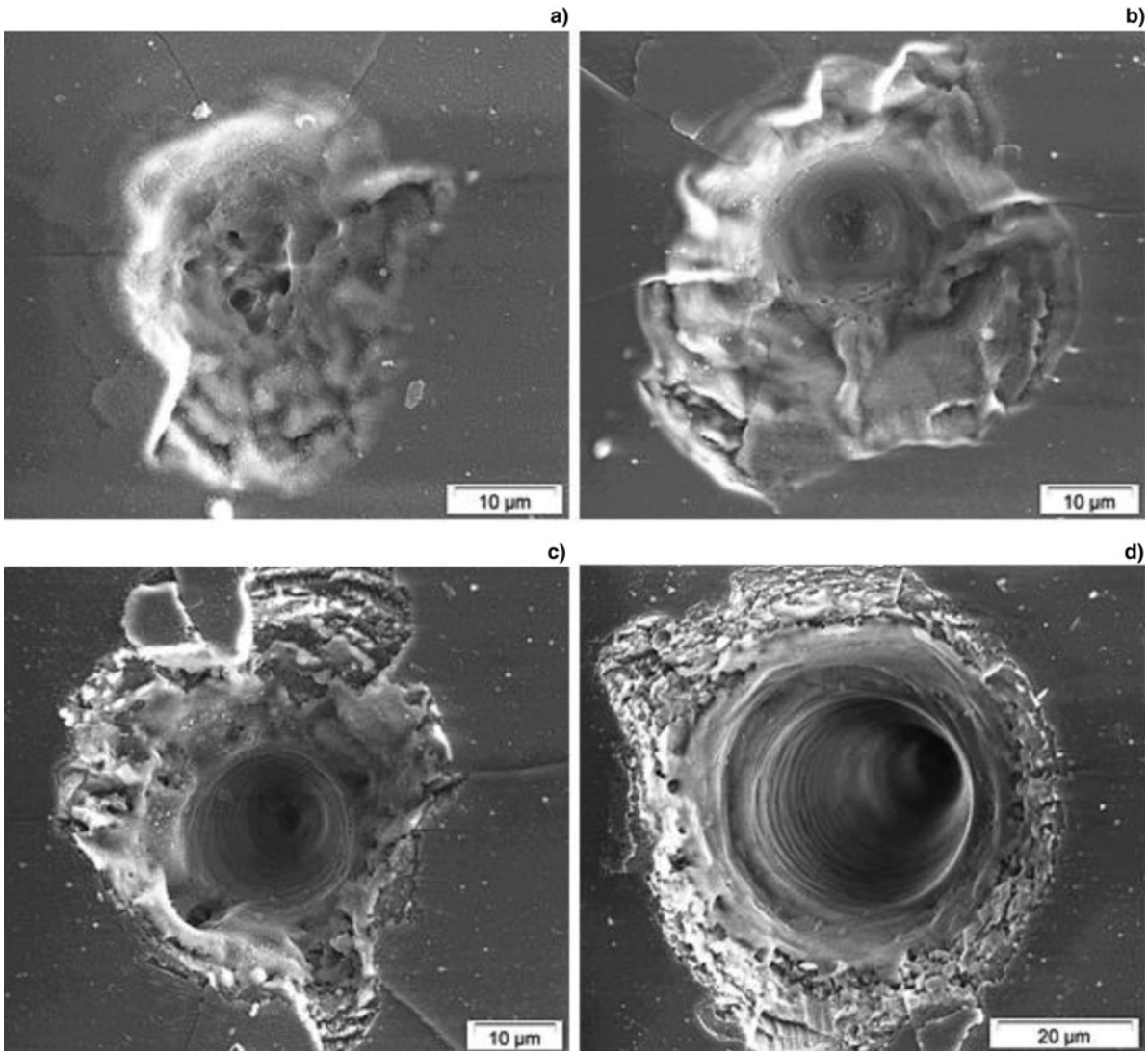


Fig. 4. Craters produced on sapphire in air using a 110 ps laser beam at a repetition rate of 100 Hz. The craters were produced using 20 (a), 50 (b), 100 (c), and 500 (d) laser pulses at fluence of 79.5 J/cm^2.

https://doi.org/10.1017/S0263034619000132 Published online by Cambridge University Press

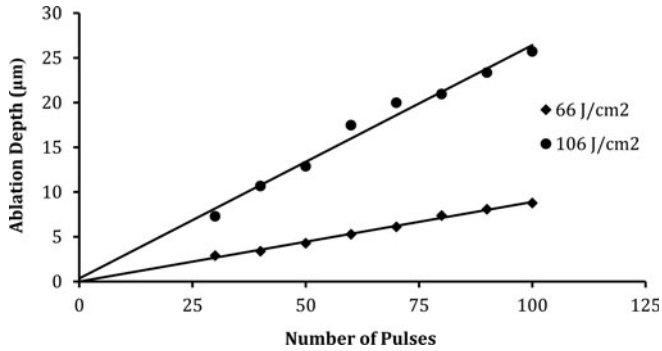


Fig. 5. Ablation depth of craters produced by picosecond laser pulses on sapphire as a function of number of laser pulses at fluence of 66 and 106 J/cm^2. Repetition rate was fixed to 100 Hz.

processes required to initiate ablation in transparent materials. Material removal or ablation starts with absorption of laser energy by free electrons (i.e., seed electrons) that are available in the interaction volume, and the subsequent transfer of energy to the lattice of the target material. The absorption mechanism of non-UV wavelengths depends on the type of the target material and on the laser intensity (Liu *et al.*, 1997). Linear absorption is the principal absorption mechanism of opaque materials when using low-intensity, long pulse-widths lasers (Liu *et al.*, 1997). In transparent materials, due to the lack of free electrons, non-linear absorption must occur to create ablation. The presence of seed electrons is essential to start ablation in transparent materials using low-intensity and low photon energy lasers. A free electron, upon absorbing the laser energy, can gain enough kinetic energy to liberate a bound electron upon collision (impact ionization)

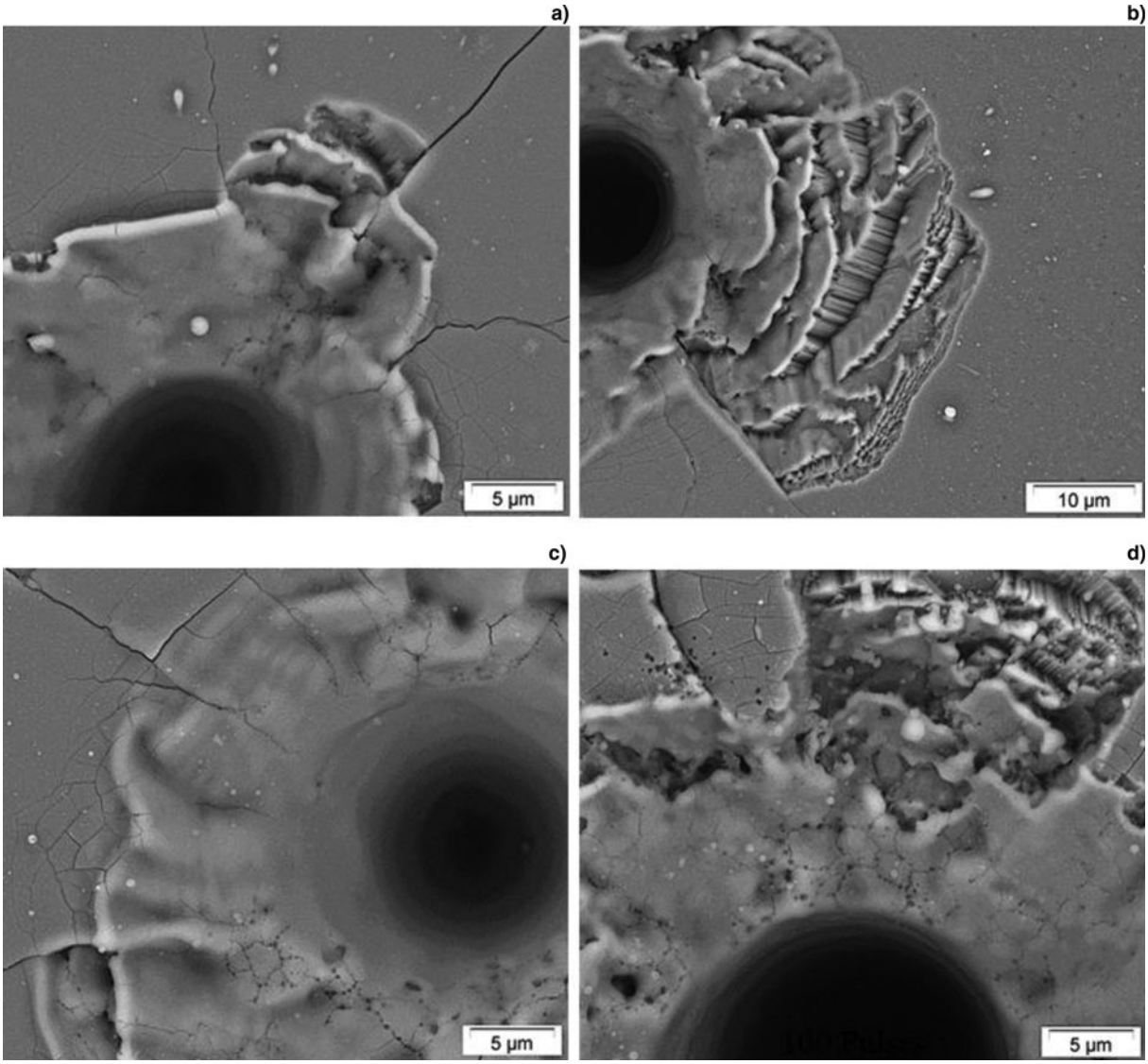


Fig. 6. Backscattered electron (BSE) images of craters produced on sapphire using 50 and 100 laser pulses at fluence of 39.8 J/cm^2 (a–b) and 79.5 J/cm^2 (c–d), respectively.

https://doi.org/10.1017/S0263034619000132 Published online by Cambridge University Press

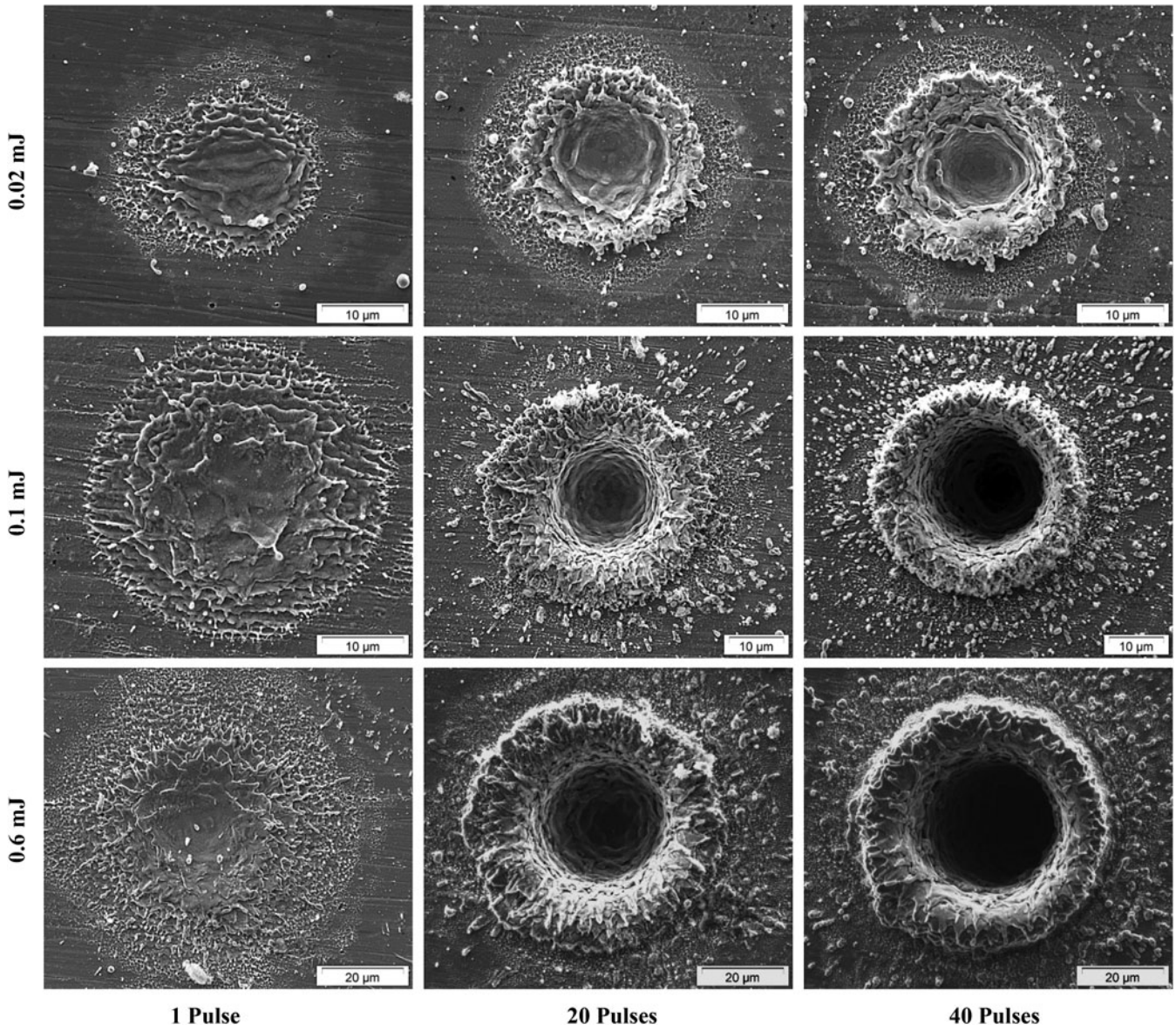


Fig. 7. SEM images of craters produced on brass in air at different fluence and number of pulses.

leading to generation of two free electrons. The two free electrons can gain enough energy to liberate another two bound electrons leading to generation of four free electrons. The process of free electron generation continues and leads to an avalanche, where the free electron density grows exponentially to reach the critical plasma density (Liu *et al.*, 1997). At this moment, the interaction volume that was initially transparent becomes an absorbing volume (Liu *et al.*, 1997). In transparent materials, seed electrons are rare and are randomly distributed over the target material. Therefore, ablation of transparent material using long-wavelength and long-pulse-width lasers is stochastic and not reproducible. It was reported that non-linear processes dominate laser–matter interaction when the laser pulse width is <10 ps (Ben-Yakar and Byer, 2004; Bäuerle, 2011; Stafe *et al.*, 2014). The laser pulse width (110 ps) used in this study was 11 times higher than this reported limit, which makes it closer to the behavior of nanosecond lasers. This explains the observed variation in the crater morphology with location on the target surface.

Figure 5 shows the dependence of ablation crater depth on the number of laser pulses at fluence of 66 and 106 J/cm^2 at a repetition rate of 100 Hz. Ablation rate (ablation depth/pulse) was calculated from the slopes of the curves in Figure 5, and was found to be 90 and 260 nm/pulse for the laser fluence of 66 and 106 J/cm^2, respectively. It was not possible to estimate ablation rates on sapphire at low fluence using light microscopy due to the limited spatial resolution of the light microscope and the low ablation rate.

A closer inspection of crater and surface morphology can reveal important information about the ablation mechanisms of transparent materials. The irregular shapes of the craters, and the development of cracks, and surface fractures observed around the craters produced on sapphire (Figs 1–4) can be attributed to the mechanical stress generated by the rapid thermal expansion of the target material (Perez and Lewis, 2002; Hu *et al.*, 2011). The energy deposition of the laser pulses into the focus volume generate thermoelastic stresses that are important in determining the characteristics of material melting, generation of defects, and ejection of

https://doi.org/10.1017/S0263034619000132 Published online by Cambridge University Press

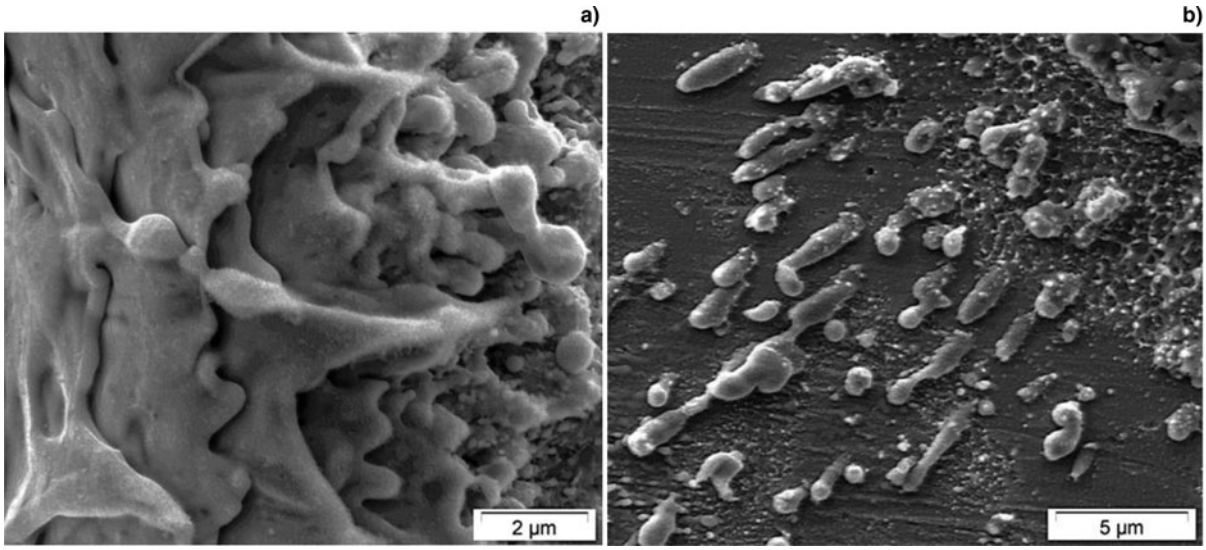


Fig. 8. A close-up image of a crater edge (a) and the particles deposited around it (b). The crater was produced on the brass at a fluence of 39.8 J/cm^2 and a repetition rate of 20 Hz.

material (Miotello and Ossi, 2010). The interaction of the laser-generated compressive stresses with the free surface of the irradiated target can generate strong tensile stresses that cause mechanical fracture, separation, and ejection of the surface layer of the brittle material (Miotello and Ossi, 2010). It is clear from Figures 3 and 4 that fracture and exfoliation of sapphire are important during ablation with picosecond laser pulses at high fluence (Vilar *et al.*, 2014). In addition to cracks and surface fractures, a few spherical particles were observed around the craters (Figs 1 and 2). These particles are re-solidified from molten material ejected from the ablated site. The presence of such spherical particles around the craters indicates that material removal has some sort of thermal nature.

Two ablation mechanisms appeared to exist at the same time when investigating the SEM images of the ablated sapphire. Thermal ablation took place predominately at the center of the crater, while fracture and exfoliation occurred at and around the crater circumference. More information can be obtained from the BSE images of the craters shown in Figure 6. The relative contribution of both mechanisms to material removal depends on fluence and number of laser pulses. Cracks and fractures of the surface were formed during the first few laser pulses. Increasing the laser fluence and number of pulses increased melting at the crater center and exfoliation at the crater edges. The fractured area around the crater decreased gradually with increasing the number of pulses due to the growth of crater volume.

The morphology of the craters produced on sapphire using picosecond laser pulses is different from that reported in a previous study using the same experimental setup but with femtosecond (130 fs) laser pulses (Shaheen *et al.*, 2015*b*). In case of femtosecond laser ablation, craters were more reproducible and easier to create using lower fluence. Cracks and surface fractures were less observed. This behavior is related to the dominance of non-linear absorption processes in femtosecond laser ablation due to the high intensity of the ultra-short laser pulses (Stuart *et al.*, 1996). The high intensity creates electrons in a process known as multi-photon ionization. This process provides seed electrons to initiate another non-linear process called avalanche ionization, which causes the electron density to reach the critical density required for material breakdown (Stuart *et al.*, 1996). Because the ablation mechanism in femtosecond laser pulses does not depend on the presence of seed electrons, which are rare and randomly distributed in transparent materials, the ablation process is deterministic with a well-defined ablation threshold and reproducible crater morphology.

Brass

Figure 7 shows SEM images of craters produced on brass using a variable number of laser pulses at a repetition rate of 20 Hz and fluence of 2.7, 13.3, and 79.5 J/cm^2. Melting and formation of liquid droplets at and around the craters were characteristics of the ablation process. This is related to the conversion of the absorbed laser energy into heat at the interaction volume. Application of a single laser pulse at low fluence (2.7 J/cm^2) led to modification of the central portion of the irradiated area and caused changes in contrast of the annular surface area surrounding it. The inhomogeneous behavior observed across the interaction area may be attributed to the variation of energy distribution across the laser beam, which has a Gaussian energy distribution. The laser energy is maximum at the beam center and the effect of the central portion of the beam is stronger than the lower energy outer edges. Increasing the number of pulses and laser fluence accumulates the effects and enhances the role of the outer area of the beam in inducing surface damage due to the accumulation of plastic deformation in the outer regions of the irradiated area (Mannion *et al.*, 2004). The crater volume was found to increase with increasing the number of pulses and the fluence due to the increased amount of material removed from the interaction volume. The accumulation and re-solidification of the molten material at the crater circumference led to the formation of craters with high rims. Figure 8 shows a high magnification SEM image of a portion of the crater rim and the particles deposited around it.

Figure 9 shows the variation in ablation rate with fluence at a repetition rate of 20 Hz. Ablation rate was found to increase from 0.2 μm/pulse at fluence of 2.7 J/cm^2 to 1.6 μm/pulse at fluence of 79.5 J/cm^2. The increase in ablation rate was not linear because the rate of ablation decreased with increasing laser fluence due to the increased loss of the incident laser energy resulting from

https://doi.org/10.1017/S0263034619000132 Published online by Cambridge University Press

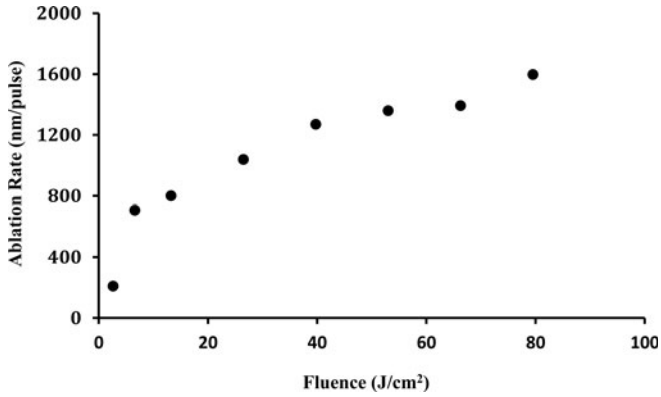


Fig. 9. Dependence of ablation rate of brass on laser fluence. Repetition rate was fixed to 20 Hz.

the interaction with the laser-induced plume, which causes absorption, reflection, and scattering of the incident laser beam. This prevents a portion of the laser energy from reaching the bottom of the crater resulting in a reduction in ablation rate. The behavior of picosecond laser interaction with brass under the conditions reported in this study (pulse with = 110 ps) is similar to that observed in nanosecond laser ablation (Shaheen and Fryer, 2012). Melting, ejection, and re-solidification of molten material and formation of craters with high edges are common in both types of laser. For laser pulses longer than the energy relaxation time (several picoseconds in metals), the energy is transferred from the laser pulse to the lattice by phonon–lattice coupling (Semerok *et al.*, 1999; Shah *et al.*, 2004). This provides a sufficient time for heating to take place during the laser pulse. At such conditions, thermal processes are the dominant mechanisms of material removal.

Conclusions

A SEM was used as a diagnostic tool to investigate the surface morphologies and mechanisms of material removal from brass and sapphire upon interaction with a 110 ps pulse-width laser beam in air at atmospheric pressure. The surface morphology was found to depend on laser fluence, number of laser pulses, and the type of target material. Exfoliation and fracture of the surface were characteristics of sapphire ablation at high fluence. Melting and ejection of molten material were also observed around the craters produced on sapphire. This morphology behavior can be attributed to the accumulation of heat during successive laser pulses and the rapid expansion of the irradiated volume, which generates internal stresses that propagate through the material causing cracks, exfoliation, and melting of sapphire. Craters produced on sapphire were not reproducible and showed morphology that varies with location on the surface. Thermal processes were dominant in picosecond laser ablation of brass, as evidenced from the SEM images of the craters where melting, ejection, and re-solidification of molten material were characteristics of the ablation process. Ablation rate of sapphire was lower than that of brass due to differences in the dissipation of laser energy in heating and fracturing of the irradiated volume. The ablation rate of brass was found to increase with fluence. The increase in ablation rate was not linear because the rate of ablation decreased with increasing laser fluence due to the increased loss of the incident laser energy caused by the interaction with the laser-generated plume.

Author ORCIDs. Mohamed E. Shaheen, 0000-0002-2906-2147.

Acknowledgments. NSERC Discovery Grants to JEG and BJF and CFI/MRI Leading Edge Funds. The authors would like to thank Sharon Lackie for her help during SEM measurements.

References

Akram M, Bashir S, Hayat A, Mahmood K, Ahmad R and Khaleeq-U-Rahaman M (2014) Effect of laser irradiance on the surface morphology and laser induced plasma parameters of zinc. *Laser and Particle Beams* **32**, 119–128.

Ali N, Bashir S, Akram M and Mahmood K (2013) Effect of dry and wet ambient environment on the pulsed laser ablation of titanium. *Applied Surface Science. Elsevier B.V.* **270**, 49–57.

Amoruso S, Ausanio G, Barone AC, Bruzzese R, Gragnaniello L, Vitiello M and Wang X (2005) Ultrashort laser ablation of solid matter in vacuum: a comparison between the picosecond and femtosecond regimes. *Journal of Physics B: Atomic, Molecular and Optical Physics* **38**, L329–L338.

Ashkenasi D, Rosenfeld A, Varel H, Wahmer M and Campbell EEB (1997) Laser processing of sapphire with picosecond and sub-picosecond pulses. *Applied Surface Science* **120**, 65–80.

Balling P and Schou J (2013) Femtosecond-laser ablation dynamics of dielectrics: basics and applications for thin films. *Reports on Progress in Physics* **76**, 036502.

Bashir S, Rafique MS, Nathala CS and Husinsky W (2013) Surface and structural modifications of titanium induced by various pulse energies of a femtosecond laser in liquid and dry environment. *Applied Physics A* **114**, 243–251.

Bäuerle D. (2011) *Laser Processing and Chemistry*, 4th Edn. Berlin, Heidelberg: Springer-Verlag.

Ben-Yakar A and Byer RL (2004) Femtosecond laser ablation properties of borosilicate glass. *Journal of Applied Physics* **96**, 5316–5323.

Brown MS and Arnold CB (2010) Fundamentals of laser-material interaction and application to multiscale surface modification in 'Laser precision microfabrication'. In Sugioka K, Meunier M and Piqué A (eds), *Laser Precision Microfabrication*, Springer Series in Materials Science. Berlin, Heidelberg: Springer, pp. 91–120.

Burakov IM, Bulgakova NM, Stoian R, Rosenfeld A and Hertel IV (2005) Theoretical investigations of material modification using temporally shaped femtosecond laser pulses. *Applied Physics A* **81**, 1639–1645.

Cui L, Wang GG, Zhang HY, Han JC, Kuang XP, Tian JL and Sun R (2014) Fabrication of nanopatterned sapphire substrates by annealing of patterned Al thin films by Laser Interference Lithography. *Applied Physics A: Materials Science and Processing* **115**, 159–165.

Dawood A, Bashir S, Akram M, Hayat A, Ahmed S, Iqbal MH and Kazmi AH (2015) Effect of nature and pressure of ambient environments on the surface morphology, plasma parameters, hardness, and corrosion resistance of laser-irradiated Mg-alloy. *Laser and Particle Beams* **33**, 315–330.

Gamaly EG, Rode AV, Luther-Davies B and Tikhonchuk VT (2002) Ablation of solids by femtosecond lasers: ablation mechanism and ablation thresholds for metals and dielectrics. *Physics of Plasmas* **9**, 949–957.

Ganeev RA (2014) *Laser Surface Interactions*. Dordrecht, Heidelberg, London, New York: Springer.

Hashida M, Semerok AF, Gobert O, Petite G, Izawa Y and Wagner JF (2002) Ablation threshold dependence on pulse duration for copper. *Applied Surface Science*. **197–198**, 862–867. Available at http://linkinghub.elsevier.com/retrieve/pii/S0169433202004634

Horisawa H, Emura H and Yasunaga N (2004) Surface machining characteristics of sapphire with fifth harmonic YAG laser pulses. *Vacuum* **73**, 661–666.

Hu H, Wang X and Zhai H (2011) High-fluence femtosecond laser ablation of silica glass: effects of laser-induced pressure. *Journal of Physics D: Applied Physics* **44**, 135202.

Hülsenberg D, Harnisch A and Bismarck A (2008) *Microstructuring of Glasses*. Berlin, Heidelberg: Springer-Verlag Berlin Heidelberg (Springer Series in Materials Science). doi: 10.1007/978-3-540-49888-9.

https://doi.org/10.1017/S0263034619000132 Published online by Cambridge University Press

Ion JC (2005) *Laser Processing of Engineering Materials*. Linacre House, Jordan Hill, Oxford: Elsevier Butterworth Heinemann.

Jelani M, Bashir S, Rehman MK, Ahamad R, Yousaf D, Akram M, Afzal N, Chaudhry M.U, Mahmood K, Hayat A and Ahmad S (2013) Effect of laser fluence on surface, structural and mechanical properties of Zr after irradiation in the ambient environment of oxygen. *The European Physical Journal D* **67**, 159.

Krstulović N, Shannon S, Stefanuik R and Fanara C (2013) Underwater-laser drilling of aluminum. *The International Journal of Advanced Manufacturing Technology* **69**, 1765–1773.

Kumar A, George S, Singh RK, Joshi H and Nampoori VPN (2011) Image analysis of expanding laser-produced lithium plasma plume in variable transverse magnetic field. *Laser and Particle Beams* **29**, 241–247.

Le Harzic R, Breitling D, Weikert M, Sommer S, Fohl C, Valette S, Donnet C, Audouard E and Dausinger F (2005) Pulse width and energy influence on laser micromachining of metals in a range of 100fs to 5ps. *Applied Surface Science* **249**, 322–331.

Lenzner M, Krüger J, Kautek W and Krausz F (1999) Incubation of laser ablation in fused silica with 5-fs pulses. *Applied Physics A Materials Science & Processing* **69**, 465–466.

Liu X, Du D and Mourou G (1997) Laser ablation and micromachining with ultrashort laser pulses. *IEEE Journal of Quantum Electronics* **33**, 1706–1716.

Mannion PT, Magee J, Coyne E, O'Connor G.M and Glynn TJ (2004) The effect of damage accumulation behaviour on ablation thresholds and damage morphology in ultrafast laser micro-machining of common metals in air. *Applied Surface Science. Elsevier* **233**, 275–287.

Miotello A and Ossi PM (eds) (2010) *Laser-Surface Interactions for New Materials Production*. Berlin, Heidelberg: Springer-Verlag.

Nedialkov N.N, Imamov S.E, Atanasov P.A, Heusel G, Breitling D, Ruf A, Hügel H, Dausinger F and Berger P (2004) Laser ablation of iron by ultrashort laser pulses. *Thin Solid Films* **453–454**, 496–500.

Perez D and Lewis L (2002) Ablation of solids under femtosecond laser pulses. *Physical Review Letters* **89**, 255504.

Qi L, Nishii K, Yasui M, Aoki H and Namba Y (2010) Femtosecond laser ablation of sapphire on different crystallographic facet planes by single and multiple laser pulses irradiation. *Optics and Lasers in Engineering. Elsevier* **48**, 1000–1007.

Semerok A, Chaleard C, Detalle V, Lacour J.-L, Mauchien P, Meynadier P, Nouvellon C, Salle B, Palianov P, Perdrix M and Petite G (1999) Experimental investigations of laser ablation efficiency of pure metals with femto, pico and nanosecond pulses. *Applied Surface* **138–139**, 311–314.

Shah L, Tawney J, Richardson M and Richardson K (2004) Self-focusing during femtosecond micromachining of silicate glasses. *IEEE Journal of Quantum Electronics* **40**, 57–68.

Shaheen ME and Fryer BJ (2012) Femtosecond laser ablation of brass: a study of surface morphology and ablation rate. *Laser and Particle Beams* **30**, 473–479.

Shaheen ME, Gagnon JE and Fryer BJ (2013*a*) Femtosecond laser ablation of brass in air and liquid media. *Journal of Applied Physics* **113**, 213106.

Shaheen ME, Gagnon JE and Fryer BJ (2013*b*) Laser ablation of iron: a comparison between femtosecond and picosecond laser pulses. *Journal of Applied Physics* **114**, 083110.

Shaheen ME, Gagnon JE and Fryer BJ (2014) Femtosecond laser ablation behavior of gold, crystalline silicon, and fused silica: a comparative study. *Laser Physics* **24**, 106102.

Shaheen ME, Gagnon JE and Fryer BJ (2015*a*) Elemental fractionation in 785 nm picosecond and femtosecond laser ablation inductively coupled plasma mass spectrometry. *Spectrochimica Acta – Part B Atomic Spectroscopy* **107**, 97–109.

Shaheen ME, Gagnon JE and Fryer BJ (2015*b*) Experimental study on 785 nm femtosecond laser ablation of sapphire in air. *Laser Physics Letters* **12**, 066103.

Shaheen ME, Gagnon JE and Fryer BJ (2016) Excimer laser ablation of aluminum: influence of spot size on ablation rate. *Laser Physics* **26**, 116102.

Shaheen ME, Gagnon JE and Fryer BJ (2019) Studies on laser ablation of silicon using near IR picosecond and deep UV nanosecond lasers. *Optics and Lasers in Engineering*. **119**, 18–25.

Stafe M, Marcu A and Puscas NN (2014) *Pulsed Laser Ablation of Solids*. In Ertl G, Lüth H and Mills DL (eds), Berlin, Heidelberg: Springer Berlin Heidelberg (Springer Series in Surface Sciences). doi: 10.1007/978-3-642-40978-3

Stuart BC, Feit MD, Herman S, Rubenchik AM, Shore BW and Perry MD (1996) Nanosecond-to-femtosecond laser-induced breakdown in dielectrics. *Physical Review. B, Condensed Matter* **53**, 1749–1761. Available at http://www.ncbi.nlm.nih.gov/pubmed/9983633.

Vilar R, Sharma SP, Almeida A, Cangueiro LT and Oliveira V (2014) Surface morphology and phase transformations of femtosecond laser-processed sapphire. *Applied Surface Science* **288**, 313–323.

von der Linde D and Sokolowski-Tinten K (2000) The physical mechanisms of short-pulse laser ablation. *Applied Surface Science* **154–155**, 1–10.

Wilder-Smith P, Lin S, Nguyen A, Liaw LH, Arrastia AM, Lee JP and Berns MW (1997) Morphological effects of ArF excimer laser irradiation on enamel and dentin. *Lasers in Surgery and Medicine* **20**, 142–148. Available at http://www.ncbi.nlm.nih.gov/pubmed/9047167

Williams DB and Carter CB (2009) *Transmission Electron Microscopy, A Text Book for Material Science*. New York, USA: Springer Science & Business Media. Available at http://linkinghub.elsevier.com/retrieve/pii/B9780128052563000040

Wu P-H, Yu X-Y, Cheng C-W, Liao C-H, Feng S-W and Wang H-C (2011) Ultrafast ablation dynamics in fused silica with a white light beam probe. *Optics Express* **19**, 16390.

Zhou Y and Wu B (2010) Experimental study on infrared nanosecond laser-induced backside ablation of sapphire. *Journal of Manufacturing Processes* **12**, 57–61.

https://doi.org/10.1017/S0263034619000132 Published online by Cambridge University Press